Synthesis and Characterization of Gyroidal Mesoporous Carbons and Carbon Monoliths with Tunable Ultralarge Pore Size

Jörg G. Werner,[†,‡] Tobias N. Hoheisel,[†] and Ulrich Wiesner[†,*]

[†]Department of Materials Science and Engineering and [‡]Department of Chemistry and Chemical Biology, Cornell University, Ithaca, New York 14850, United States

ABSTRACT Ordered mesoporous carbons with high pore accessibility are of great interest as electrodes in energy conversion and storage applications due to their high electric and thermal conductivity, chemical inertness, and low density. The metal- and halogen-free synthesis of gyroidal bicontinuous mesoporous carbon materials with uniform and tunable pore sizes through bottom-up self-assembly of block copolymers thus poses an interesting challenge. Four double gyroidal mesoporous carbons with pore sizes of 12, 15, 20, and 39 nm were synthesized using poly(isoprene)-*block*-poly(styrene)-*block*-poly(ethylene oxide) (ISO) as structure-directing triblock terpolymer and phenol–formaldehyde resols as carbon precursors. The highly ordered materials were thermally stable to at least 1600 °C with pore volumes of up to 1.56 $cm^3\ g^{-1}$. Treatment at this temperature induced a high degree of sp^2-hybridization and low microporosity. Increasing the resols/ISO ratio led to hexagonally packed cylinders with lower porosity. A single gyroid carbon network with high porosity of 80 vol % was obtained using a similar synthesis strategy. Furthermore, we present a method to fabricate monolithic materials of the gyroidal carbons with macroscopic shape and thickness control that exhibit an open and structured surface with gyroidal features. The gyroidal materials are ideally suited as electrode materials in fuel cells, batteries, and supercapacitors as their high, three-dimensionally connected porosity is expected to allow for good fuel or electrolyte accessibility and to prevent total pore blockage.

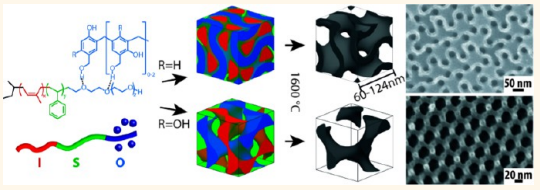

KEYWORDS: phenolic resols–triblock terpolymer co-assembly · monolithic ordered mesoporous carbon · gyroidal mesoporous carbon · ultralarge pore size · high thermal stability

Chemical and physical properties like good electrical and thermal conductivity, chemical resistance, and inertness as well as low density combined with high surface area and porosity make porous carbon materials a preferred material in a broad field of applications, such as electrodes in batteries and fuel cells and gas adsorbents.[1−3] Ordered mesoporous carbons (OMCs) have retained a lot of attention since their first synthesis in 1999, where silica templates were used as a mold.[4,5] This hard-templating method is very versatile, and dimensions are only limited by the availability of the silica template, but it is tedious due to multiple step synthesis and the removal of the silica template with hazardous chemicals.[6−12] In 2004, Liang *et al.* reported the first soft-templated OMC.[13] They used structure direction from the block copolymer poly(styrene)-*block*-poly(4-vinylpyridine) (PS-*b*-P4VP) with resorcinol through solvent evaporation induced self-assembly (EISA) and subsequent gas–solid reaction with gaseous formaldehyde. The resulting carbon thin films of up to 1 μm thickness showed hexagonally ordered cylindrical pores with a pore size of 33.7 nm after pyrolysis. Since this first report, extensive studies on soft-templated OMCs have been performed using the surfactant-like block copolymers Pluronics. Due to the small molar mass of these structure-directing molecules, however, the accessible pore size range was limited to less than 4 nm, which was increased to 15–16 nm by molecular swelling agents, as well as by using carbon onions or carbon black additives.[14−17] Only a few reports on the use of block copolymers with molar masses up to 45.6 kDa for the synthesis of OMCs with larger pore sizes were published.[18−21] Pore sizes up to 37 nm have been achieved using poly(styrene)-*block*-poly(ethylene oxide) (PS-PEO)

* Corresponding author: ubw1@cornell.edu.

Received for review October 16, 2013 and accepted December 11, 2013.

Published online December 11, 2013
10.1021/nn405392t

© 2013 American Chemical Society

with poly(styrene) homopolymer addition as pore expander and phenolic resols as the carbon precursors.[23] The mesostructures achieved with these polymers were inverse micellar and hexagonally packed cylinders. Ordered, bicontinuous networks, such as gyroidal mesoporous carbons, have only been reported using Pluronics and recently using the structure-directing block copolymer poly(ethylene oxide)-*block*-poly-(ε-caprolactone) (PEO-*b*-PCL).[15,22] However, the reported material showed only a small pore size of 11 nm and low porosity.

Here we report the tunable synthesis of two gyroidal mesoporous carbon (G^DMC and G^AMC) morphologies through the EISA process of the structure-directing triblock terpolymer poly(isoprene)-*block*-poly(styrene)-*block*-poly(ethylene oxide) (ISO) with phenol– or resorcinol–formaldehyde resols as carbon precursors. We demonstrate the tunability of the materials' characteristics such as porosity, pore size, and mesostructure by rational design of the soft template. Organic–organic hybrids with the core–shell double gyroid and hybrids with the alternating gyroid morphology result in a double gyroidal carbon matrix and a single gyroidal carbon network after pyrolysis, respectively. Pore tunability was achieved through variation of the triblock terpolymer composition and the respective polymer to resols ratios. The pore size tunability is demonstrated by using three ISOs with similar composition but different molar mass. The bicontinuous, ordered carbon materials show surprisingly good structure retention after heat treatment at temperatures as high as 1600 °C. This high-temperature stability allows for thermal tunability of the microstructure of the carbon as well as the microporosity. A report by Wang *et al.* showed the retention of only local order of a hexagonally packed cylindrical carbon mesostructure at 1800 °C with structural collapse at higher temperatures by scanning electron microscopy.[24] However, the long-range order of the material treated at these high temperatures was not retained according to small-angle X-ray scattering (SAXS). For the ordered gyroidal mesoporous carbons reported here, up to six clearly identifiably SAXS peaks remained, demonstrating, for the first time, long-range order retention at 1600 °C.

Much research in electrochemical energy storage focuses on the enhancement of rate capability during charge and discharge of supercapacitors and batteries. Due to better electrolyte accessibility and shorter solid-state diffusion length, nanoporous materials have been proven to enhance the rate of charge and discharge while keeping the capacity loss small. However, the standard device design of these electrochemical devices employs powders of the active materials and conductive additives, held together in a film by a polymeric binder. The contact resistance between the micrometer-sized particles causes large ohmic losses, especially at high-frequency operations. Therefore,

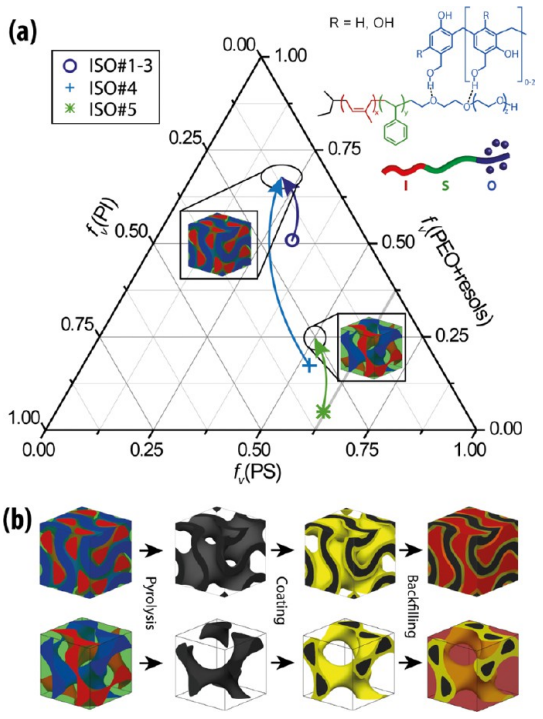

Scheme 1. (a) Ternary volume fraction phase portrait that shows the reported ISO triblock terpolymer compositions and gyroidal hybrid compositions after incorporation of resols into the PEO block of the terpolymers. Inset shows the proposed mechanism of formation of resols–ISO organic–organic hybrids through self-assembly of the hydrogen-bonded assembly. (b) Illustration of gyroidal structures and formation of gyroidal mesoporous carbon networks through decomposition of the triblock terpolymer and pyrolysis of the carbon precursor. The coating and backfilling steps are proposed routes to convert the carbon networks into two- and three-component functional nanocomposites. Top row: formation of core–shell double gyroid structure. Bottom row: formation of alternating gyroid structure.

monolithic electrodes without particle-to-particle resistance are highly desirable for future energy storage devices. There are several reports in the literature for ordered mesoporous monolithic carbon materials, usually by hard-templating.[12] Two soft-templating approaches have also been described, that is, hierarchical macro-mesoporous carbon monoliths from hydrothermal synthesis and EISA.[25–29] The macropores and only micrometer-sized mesoporous walls in the hierarchical carbons ensure sufficient release pathways for the decomposition gases and good strain relaxation upon carbonization. In the EISA-derived monoliths, carbon–silica composites have been employed. The mechanically robust silica prevents collapse of the monolith during carbonization, but it makes the undesirable extra step of silica removal necessary.[30] These monoliths are typically irregular with ill-defined macroscopic structure, and they exhibit unstructured surfaces with broad pore size distributions. In contrast, here we present a silica-free soft-templating method to produce well-defined, ordered, purely mesoporous carbon monoliths with tunable macroscopic dimensions.

TABLE 1. Triblock Terpolymer Compositions and Resols Loadings for Gyroidal Organic–Organic Hybrids

polymer	GMC	M_N[a] (g/mol)	PDI	f_V(PI)[b] (vol %)	f_V(PS)[b] (vol %)	f_V(PEO)[b] (vol %)	resols/ISO[c]
ISO#1	G^DMC#1–15	38891	1.06	17.7	32.5	49.8	0.58:1
ISO#2	G^DMC#2–20	55993	1.06	16.7	31.2	52.1	0.73:1
ISO#3	G^DMC#3–39	108311	1.07	17.7	31.6	50.7	0.50:1
ISO#4	G^DMC#4–12	27019	1.05	30.1	52.6	17.3	1.80:1
ISO#5	G^AMC#5	68959	1.04	33.1	62.0	4.9	0.32:1

[a] Determined by combination of ^{1}H NMR and GPC. [b] Determined by ^{1}H NMR. [c] Weight ratio.

Furthermore, we report a process to achieve surfaces with narrow pore size distributions that exhibit the same ordered gyroidal features as the bulk of the material.

RESULTS AND DISCUSSION

Characterization of Mesostructure. The formation of mesoporous carbon materials by block copolymer structure direction of phenol– or resorcinol–formaldehyde carbon precursors is illustrated in Scheme 1. Five poly(isoprene)-*block*-poly(styrene)-*block*-poly(ethylene oxide) (ISO) terpolymers with polydispersity indices of 1.04–1.07 (Table 1) were synthesized using anionic polymerization to serve as the soft template for the preparation of gyroidal mesoporous carbon structures by evaporation-induced self-assembly (EISA). Briefly, in this process, a solution of the carbon precursor and the terpolymer template is slowly evaporated to dryness, leading to microphase separation of the block terpolymer. The hydrophilic carbon precursor forms hydrogen bonds with the hydrophilic poly(ethylene oxide) (PEO) block of the terpolymer, which ensures that the carbon precursor is embedded in the PEO block, selectively swelling this phase.[33] The organic–organic hybrid film is subsequently annealed to cure the resols. Further heat treatment under inert atmosphere condenses the resols to a highly cross-linked resin, while the block copolymer decomposes (Scheme 1 and Figure 2a), yielding an ordered gyroidal mesoporous polymeric resin. Pyrolysis at temperatures above 600 °C leads to carbonization of the resin to form the desired gyroidal mesoporous carbons with tailored porosity and pore sizes.

During the EISA process, microphase separation occurs when a critical concentration of the polymer/additive is reached in the solution. This process is very sensitive to both the processing parameters and the precursor molecules employed. First, well-defined mesostructures only form in systems in which the different blocks have sufficiently high Flory–Huggins interaction parameters.[38] Second, it is critical to ensure strong and selective hydrogen bonding between the resols and the PEO for selective swelling of this block. The morphology that is formed depends on the volume fractions of the separated microphases and their interaction parameters. With decreasing amount of solvent, the mobility of the polymer decreases until it reaches a kinetically trapped state. If the additive, in this case the resols, is not bonded strongly enough to one of the polymer blocks, the interface between the hydrophilic and hydrophobic phases is unsharp. This leads to unstructured microphase separation or poor structure formation and no long-range order. In order to form well-defined gyroidal organic–organic hybrids, the solvent system and precursors as well as the mixing time and casting temperature had to be optimized. While protocols reported in the literature for block copolymer–resols structure direction[19–21] resulted in limited structure formation and order (Supporting Information Figure S1a), optimization of the above-mentioned parameters yielded well-defined organic–organic ISO–resols hybrids (Figure 2b), highlighting the importance of the conditions for film-casting. In our case, the desired gyroidal morphology was only achievable using a casting solution stirred for 24 h in a solvent system of tetrahydrofuran (THF) and chloroform and elevated casting temperatures for solvent evaporation (Figure 2b–f). Third, to ensure structural stability of the ordered nanomaterial during decomposition of the triblock terpolymer template, high enough loading of the cross-linkable precursor is crucial in soft-templating methods, as opposed to hard-templating methods. On the other hand, high porosity and large specific surface areas are desirable for most applications, favoring lower loadings. We specifically designed our triblock terpolymers with different compositions to ensure thermal stability and structural integrity through sufficient connectivity of the carbon precursor while yielding tunable porosities between 32 and 80 vol %.

Double Gyroidal Mesoporous Carbon (G^DMC). Three triblock terpolymers, ISO#1–ISO#3, with a PEO volume fraction of approximately 50 vol % and molar mass of 39 kDa (ISO#1), 56 kDa (ISO#2), and 108 kDa (ISO#3), and a fourth triblock terpolymer ISO#4, with a PEO volume fraction of 17 vol % and a molar mass of 27 kDa, were used for the preparation of ordered mesoporous carbons (OMCs) with double gyroid morphology (Q^{230}, $Ia\bar{3}d$) (Table 1 and Scheme 1a). These materials were designated G^DMC#X-Y-Z, where X represents the terpolymer number, Y the approximate final pore size, and Z the highest temperature at which the material was heat-treated. In the organic–organic hybrid, the hydrophilic phase, consisting of PEO and resols, formed the matrix that separates the two interpenetrating gyroidal poly(isoprene)-*block*-poly(styrene) core–shell networks (top row in Scheme 1b). In Figure 1, the well-resolved small-angle X-ray patterns of the hybrids are shown (lowest trace in each graph). For hybrids from polymers ISO#1, ISO#2, and ISO#4, multiple higher order peaks consistent with the space group Q^{230} were

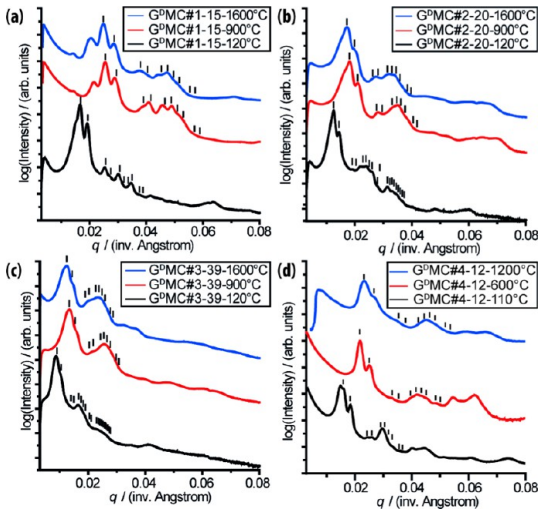

Figure 1. Small-angle X-ray scattering patterns of double gyroidal organic−organic hybrids and double gyroidal mesoporous carbons: (a) $G^DMC#1-15$, (b) $G^DMC#2-20$, (c) $G^DMC#3-39$, and (d) $G^DMC#4-12$. Black traces after curing at 110−120 °C, red traces after pyrolysis at (a−c) 900 °C and (d) 600 °C, and blue traces after pyrolysis at (a−c) 1600 °C and (d) 1200 °C. The vertical ticks in the SAXS patterns indicate the expected peak positions of the double gyroid lattice (Q^{230}).

observed, indicating a high degree of long-range order. The SAXS pattern for the hybrid obtained from the largest terpolymer ISO#3 showed a broad first-order peak with a shoulder on the higher *q* side together with broad higher order peaks, making structural assignments based on SAXS data only challenging. The lower resolution of the SAXS pattern for this hybrid as compared to the SAXS patterns of the hybrids from ISO#1, ISO#2, and ISO#4 is due to squeezing of all reflexes into a smaller *q* range as well as a decreased degree of long-range order, as expected for a higher molar mass polymer. In the EISA process, as the solvent evaporates, the hybrids self-assemble into their structures once a certain concentration is reached. During this self-assembly, the solvent swells the polymer and, therefore, provides mobility to the polymer chains. When the solvent concentration drops, the system starts to freeze since the casting temperature is below the glass-transition temperature of the poly(styrene) block. Casting or thermal annealing at temperatures higher than the glass-transition temperature of poly(styrene) is not possible because it would induce cross-linking of the phenolic resols. Higher molar mass polymers have lower mobility and, therefore, yield smaller grain sizes and lower long-range order than smaller molar mass structure-directing polymers. Therefore, the best resolved SAXS patterns are obtained with the smallest triblock terpolymers ISO#1 and ISO#4. Moreover, the different molar masses of the three ISO polymers with similar composition, ISO#1−3, resulted in different characteristic structural length scales of the prepared hybrids. A clear trend of the first-order peak that corresponds to the (211) plane of the Q^{230} space group to lower *q* values was observed when comparing the patterns for $G^DMC#1-15-120$, $G^DMC#2-20-120$, and $G^DMC#3-39-120$. This decrease corresponds to an increase in the unit cell size of the cubic morphology from 92 to 123 nm to 169 nm for hybrids of ISO#1, ISO#2, and ISO#3, respectively, as expected from the increasing molar mass of the three structure-directing triblock terpolymers. The organic−organic hybrid of ISO#4 and resols gave a gyroidal unit cell size of 96 nm, only 4% larger than $G^DMC#1-15-120$. Even though ISO#4 has a 31% smaller molar mass with a more than two times lower PEO fraction than ISO#1, the three times higher resols loading of $G^DMC#4-12$ made the two hybrids very comparable in composition of the three phases, PI, PS, and PEO−resols. This leads to two double gyroidal materials with similar characteristic length scales but significantly different compositions of the hydrophilic PEO−resols phase; that is, $G^DMC#4-12$ has a much higher resols/PEO ratio than $G^DMC#1-15$ (Scheme 1a).

The hybrids were subsequently heated under inert atmosphere to decompose the terpolymer and carbonize the resols. First, the hybrids were heated to 600 °C at a rate of 1 °C min^{-1} and held at that temperature for 3 h to ensure sufficient structure stabilization. For further carbonization, two temperatures were investigated: 900 °C for 3 h, often employed in literature reports of mesoporous carbons, and 1600 °C for 1 h; both temperatures were reached with a heating rate of 5 °C min^{-1}.[19] Upon heat treatment and carbonization, the structure shrinks significantly but is well-retained. This is apparent from the well-resolved SAXS patterns that, compared to the parent hybrids, were shifted to higher *q* values corresponding to smaller unit cell sizes but retained higher order reflections consistent with a cubic gyroid lattice (middle and upper traces in Figure 1a−d and Table 2). According to the decrease of the unit cell, the structures shrank approximately 30% during decomposition of the polymer and carbonization of the resols. Considering this large change in size, the thermal stability of the mesostructure of these materials is remarkable. To the best of our knowledge, this is the first report of soft-templated materials with long-range-ordered and periodic mesostructure after treatment at temperatures as high as 1600 °C. The lack of an appropriate furnace inhibited further exploration of the thermal stability at even higher temperatures of these materials. It is noteworthy that the shrinkage of the structure during heat treatment at 900 °C (for 3 h) was larger than during the heating at 1600 °C (for 1 h). We assume that, after the stabilization at 600 °C, the phenolic resin condensed very slowly. A temperature plateau at 900 °C could allow the mesostructure to relax or condense for a longer time compared to material that is directly heated to 1600 °C and hardened quickly. Additionally, for ISO#1-derived

TABLE 2. Structural Characteristics of Gyroidal Mesoporous Carbons

GMC	pore size[a] (nm)	pore volume,[b] cm^3/g (micropore volume,[c] cm^3/g)	BET surface area, m^2/g (micropore area,[c] m^2/g)	*d*-spacing[d] (nm)	carbon/oxygen ratio[e]	graphitic cluster size[f] (Å)
G^DMC#1−15−900	15 ± 2	0.89 (0.2)	606 (427)	60	88:12	26.8 ± 3.0
G^DMC#1−15−1600	16 ± 2	0.80 (0.06)	318 (136)	62	91:9	37.4 ± 3.0
G^DMC#2−20−900	19 ± 2	0.78 (0.19)	551 (403)	86	88:12	27.0 ± 4.1
G^DMC#2−20−1600	21 ± 2	0.80 (0.03)	196 (72)	89	92:8	37.6 ± 2.1
G^DMC#3−39−900	39 ± 4	1.56 (0.23)	692 (506)	116	85:15	27.2 ± 2.4
G^DMC#3−39−1600	39 ± 5	1.15 (0.03)	202 (74)	124	90:10	36.9 ± 4.0
G^DMC#4−12−900	11 ± 2	0.37 (0.2)	529 (437)	71[g]	80:20	27.1 ± 1.0
G^DMC#4−12−1600	12 ± 3	0.24 (0.06)	172 (93)	66[h]	86:14	34.2 ± 2.2
G^AMC#5−900	35 ± 5	2.01 (0.15)	588 (332)	48	90:10	29.6 ± 3.1
G^AMC#5−1600	31 ± 9	1.41 (0.05)	348 (120)	49	93:7	36.7 ± 5.7

[a] Determined by BJH model applied to nitrogen sorption isotherms. [b] Based on amount adsorbed at relative pressure of 0.99. [c] Determined using the *t*-plot method. [d] Determined by SAXS. [e] Determined by XPS. [f] Determined by fitting of Raman spectra. [g] From G^DMC-12−600. [h] From G^DMC-12−1200.

G^DMC#1−15, the SAXS patterns after heat treatment showed an extra peak at lower *q* values. The peak matched the (200) peak that is forbidden in the cubic double gyroid morphology. This suggests anisotropic shrinkage of the structure during heat treatment as has been observed for oxide materials in the past.[36] The SAXS pattern of G^DMC#4−12−600 shows multiple higher order peaks consistent with the double gyroid morphology. After heat treatment at 1200 °C, the peaks broadened. The gyroidal unit cell of the ISO#4−resols hybrid shrank from 96 to 71 nm and 66 nm after pyrolysis at 600 and 1200 °C, respectively. The characteristic length scale of G^DMC#4−12−1200 and G^DMC#1−15−1600 only differed by 8%.

The remarkable structure control as evidenced by SAXS and the assignments to gyroidal structures in all four materials was corroborated by scanning electron microscopy (SEM) (see Figure 2c−f). The SEM images show the well-defined (211) projection (double wavy pattern) of the double gyroid morphology for all four materials. The extensive long-range order of GDMC#1−15−1600, apparent from the well-resolved SAXS pattern, was also evident from electron microscopy analyses. Grains with diameters of multiple micrometers were seen in SEM images that were connected by thin lamellae grain boundary regions. During crushing of the samples, the grain boundaries are mechanically the weakest points of the structure, and mesostructurally "single-crystalline" particles with sizes of more than 5 μm were observed in TEM (Figure S2). While electron microscopy analysis indicated a low porosity for the G^DMC#4−12−1200 materials derived from ISO#4 with low PEO fraction and high resols loading, a high porosity was suggested for the materials derived from ISO#1−3 with high PEO fractions and low resols loadings. Thus, the thickness of the pore walls of the latter three investigated double gyroidal mesoporous carbons were measured to be between 10 and 15 nm with wall-to-wall distances of approximately 15, 19, and 36 nm for G^DMC#1−15−1600, G^DMC#2−20−1600, and G^DMC#3−39−1600, respectively (see insets in Figure 2d−f). In contrast to these high pore-to-wall thickness ratios, the wall thickness and wall-to-wall distance of G^DMC#4−12−1600 were measured to be 20 and 12 nm, respectively.

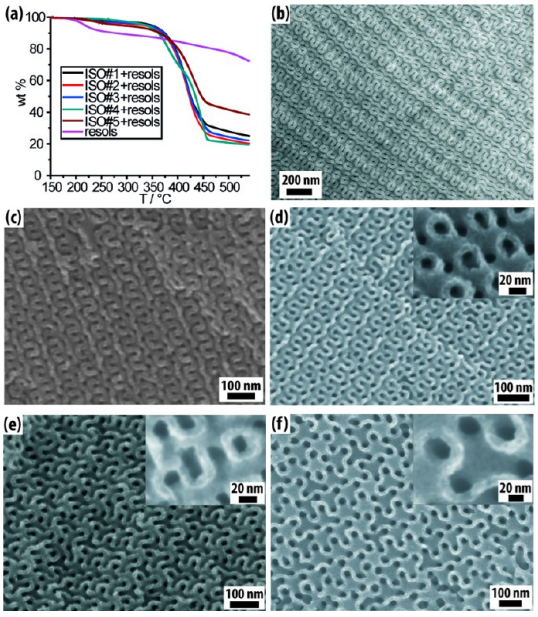

Figure 2. (a) Thermogravimetric analysis curves of all five reported ISO−resols hybrids and pure phenol/formaldehyde resols. (b) Transmission electron micrograph of ISO#2−resols hybrid stained with osmium tetroxide (selectively stains poly(isoprene)), showing the double gyroidal (211) plane. Scanning electron microscopy images of (c) GDMC#4−12−1600, (d) GDMC#1−15−900, (e) GDMC#2−20−900, and (f) GDMC#3−39−1600. Insets show images taken at higher magnification to demonstrate the difference in pore size and similarities in wall thickness between the three double gyroidal carbon materials derived from ISO#1−3.

Nitrogen sorption analysis of the carbonized samples confirmed the presence of mesoporous structures with narrow pore size distributions and tunable porosity. Figure 3a shows nitrogen sorption isotherms of all four G^DMCs pyrolyzed at 1600 °C. The isotherms show typical type-IV curves with H_1-type hysteresis and

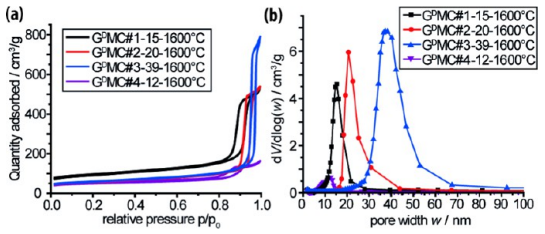

Figure 3. (a) Nitrogen sorption isotherms and (b) pore size distributions of GDMC#1−15−1600, GDMC#2−20−1600, GDMC#3−39−1600, and GDMC#4−12−1600. The pore size distributions were calculated using the BJH model for cylindrical pores.

sharp capillary condensation above relative pressures of 0.9. The sharp capillary condensation shifted to higher relative pressures with increased molar mass of the terpolymer template. The amount of nitrogen adsorbed at low relative pressure was twice as high for the carbon materials treated at 900 °C (Figure S1b) compared to the ones treated at 1600 °C, indicating a much higher specific surface area. Analysis according to the Brunauer−Emmett−Teller (BET) theory resulted in specific surface areas of 529, 606, 551, and 692 $m^2\ g^{-1}$ for G^DMC#4−12−900, G^DMC#1−15−900, G^DMC#2−20−900, and G^DMC#3−39−900, respectively (Table 2). More than two-thirds of these specific surface areas were constituted by microporosity. However, pyrolysis of the mesoporous carbons at 1600 °C resulted in a large decrease of the contribution of the micropores to the specific surface area, while the mesopore surface area (obtained through subtraction of the micropore surface area from the total surface area) remained almost unchanged (Table 2). At this temperature, the micropore surface area only contributed 27−30% to the total surface area of G^DMC#1−15−1600, G^DMC#2−20−1600, and G^DMC#3−39−1600, while micropores still contributed 54% to the total surface area for G^DMC#4−12−1600, indicating a relation between the carbon wall thickness and microporosity. Nitrogen sorption also confirmed the high porosity for the ISO#1−3-derived materials, supporting the results from SEM analysis. Assuming a carbon density of 2 g cm^{-3}, a porosity of 62% was calculated from the pore volumes of around 0.8 $cm^3\ g^{-1}$ for G^DMC#1−15−1600 and G^DMC#2−20−1600. With a pore volume of 1.2 $cm^3\ g^{-1}$, G^DMC#3−39−1600 exhibited a high porosity of 71%, even after heat treatment at 1600 °C. By comparison, G^DMC#4−12−1600 displayed a significantly lower porosity of 32 vol % as a result of the high content of carbon precursor in the hybrid, which was necessary to achieve the double gyroid morphology from the low PEO content in ISO#4. This demonstrates the tunability of the porosity of the carbon materials by changing the PEO content of the starting polymer. The tunability of the pores was further evidenced by comparing the contributions of micro- and mesopores to the pore volume of the G^DMC materials pyrolyzed at 1600 °C. For materials derived from ISO#1−3, the microporosity decreased drastically due to extensive condensation, and its contribution to the pore volume was minimal (Table 2). In most porous carbon materials with high porosity, pores of less than 5 nm diameter make up the majority of the pore volume.[15] In contrast, the large mesopores contributed over 96% of the pore volume in the G^DMC#1−15−1600, G^DMC#2−20−1600, and G^DMC#3−39−1600 materials. The tremendously high-temperature stability of the ordered structure of the carbon materials made this high mesoporosity with low microporosity possible. For G^DMC#4−12−1600, the micropores still contributed 25% to the total pore volume, showing again that the ratio of micro- and mesoporosity seems to be dependent on the pore wall thickness at these high pyrolysis temperatures.

Analysis of the nitrogen adsorption isotherm using the Barrett−Joyner−Halenda (BJH) method resulted in narrow pore size distributions centered at 12, 16, 21, and 39 nm for G^DMC#4−12−1600, G^DMC#1−15−1600, G^DMC#2−20−1600, and G^DMC#3−39−1600, respectively (Figure 3b), consistent with the SEM analysis. To the best of our knowledge, the ultralarge pore size of 39 nm is the largest reported to date for ordered soft-templated carbon materials. It exceeds the largest pore size previously reported, face-centered cubic packed spherical pores, by 5% and the largest reported gyroidal mesoporous carbon by more than 300%. This demonstrates the versatile tunability over a wide range of structural and porosity characteristics by rational design of the structure-directing block copolymer.

Alternating Gyroidal Mesoporous Carbon (G^AMC). Another cubic bicontinuous morphology that is thermodynamically stable for triblock terpolymers is the so-called alternating gyroid (Q^{214}, $I4_132$).[37] In this morphology, the PI and the PEO end blocks each form a single gyroid network in a PS matrix. The two chemically distinct networks are enantiomeric and interpenetrating (Scheme 1). For the fabrication of G^AMC#5, we synthesized the terpolymer ISO#5 with a very low PEO volume fraction of 4.9 vol % and a low polydispersity of 1.04 (Table 1). Following the protocol described above for the successful and well-controlled synthesis of double gyroidal organic−organic hybrids, however, we were not able to obtain ordered hybrids using ISO#5 and phenol−formaldehyde resols (Figure S3). In order to increase the interaction parameter between the hydrophilic and hydrophobic phases in our mixed polymer/resols system, we introduced more phenolic hydroxy groups by using resorcinol−formaldehyde resols as the carbon precursor. This change in precursor functionality led to the formation of organic−organic hybrids with well-ordered network morphology following our protocol, which was subsequently converted into an OMC network by pyrolysis.

The SAXS pattern of the organic−organic hybrid from ISO#5 and resorcinol−formaldehyde resols showed

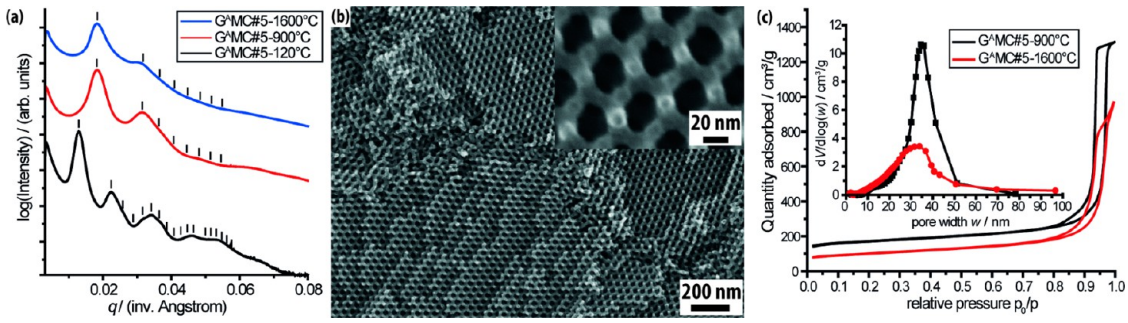

Figure 4. (a) Small-angle X-ray scattering patterns, (b) scanning electron microscopy image (inset: higher magnification of the (111) projection) after pyrolysis at 1600 °C, and (c) nitrogen sorption isotherms with BJH pore size distributions (inset) of alternating gyroidal mesoporous carbons (G^AMC#5).

multiple peaks, some of which were overlapping (black trace in Figure 4a). The first sharp peak at a q value of 0.13 $Å^{-1}$ was followed by a peak at 0.2 $Å^{-1}$ with a shoulder on the higher q side and a third peak at 0.35 $Å^{-1}$ with a shoulder on either side. The peaks and their shoulders matched the q/q^* ratios of $\sqrt{3}$, $\sqrt{4}$, $\sqrt{6}$, $\sqrt{7}$, and $\sqrt{8}$, with q^* being the first-order peak, consistent with the allowed peaks of the Q^{214} space group. Note that an expected peak at a ratio of $\sqrt{5}$ to the first-order peak did not appear. However, the existence of the peak with a q/q^* ratio of $\sqrt{6}$, corresponding to the (222) plane, and the absence of a peak with a $\sqrt{2}$ ratio suggested the formation of the alternating gyroid structure in the organic–organic hybrid. The first peak at 0.13 $Å^{-1}$ corresponds to the (110) plane of the alternating gyroid morphology with a lattice constant of 69 nm.

Upon heat treatment under inert atmosphere, the resorcinol–formaldehyde resols–ISO hybrid was converted into a periodically ordered mesoporous carbon network. The SAXS patterns after pyrolysis shifted to higher q values and exhibited a lower resolution, in contrast to the double gyroidal mesoporous carbons. This was probably due to the fragility of the single gyroid network that caused nonuniform shrinkage and loss of symmetry. However, a first-order peak and a higher order peak with a shoulder on the high q side were clearly distinguishable. The q/q^* ratio of the peaks and the shoulder were 1, $\sqrt{3}$, and $\sqrt{4}$, consistent with the (110), (211), and (220) plane reflections of the Q^{214} space group with $I4_132$ symmetry. However, the gyroidal morphology might not be completely retained after pyrolysis, and formation of a structure only closely related to the single gyroidal morphology is also possible.[31] The resolution of the pattern was independent of the pyrolysis temperature. The decrease in unit cell size of the material before and after heat treatment corresponded to a 30% shrinkage of the periodic single network, very similar to the shrinkage seen in the case of the double gyroidal morphology. To the best of our knowledge, this is the first report of a single gyroidal mesoporous carbon network.

Scanning electron microscopy of the pyrolyzed G^AMC#5 supported the formation of a well-ordered and periodic, porous single gyroidal network. The highly ordered network that was observed exhibited thin struts that were connected by triple nodes (Figure 4b). At higher magnification, a honeycomb-like structure with two struts per hexagon coming out of the image plane that matches the (111) projection of a single gyroid network was seen (inset in Figure 4b). From analysis of the SEM images, the diameter of the struts was determined to approximately 15 nm, and the pore diameter along the (111) projection was determined to approximately 26 nm. Similar to the SAXS patterns, the order that was seen in the SEM images did not change when the pyrolysis temperature was increased from 900 to 1600 °C as evidenced by a similar grain size of the mesostructure on the order of a few micrometers for materials heated to these temperatures. Considering the low carbon precursor content in the organic–organic hybrid, it is astonishing that the ordered morphology does not collapse upon decomposition of the structure-directing triblock terpolymer and excessive condensation of the resin during carbonization at temperatures as high as 1600 °C. The SEM images suggest a very high porosity of the single gyroidal carbon network, which is expected from the low resorcinol–formaldehyde resols to ISO ratio, with good structure retention.

Nitrogen sorption confirmed the high porosity of the single gyroidal carbon network (Figure 4c). For both heat treatment temperatures, the isotherms showed typical type-IV curves with H_1-type hysteresis and sharp capillary condensation above relative pressures of 0.95. The amount of nitrogen adsorbed at low relative pressure was almost twice as high for the sample treated at 900 °C compared to the one heated to 1600 °C, indicating a much higher specific surface area for the lower-temperature-treated carbon network. BET analysis resulted in specific surface areas of 588 and 348 $m^2\ g^{-1}$ for G^AMC#5–900 and G^AMC#5–1600, respectively. The micropore surface area contributed more than 50% to the total surface area for samples heated at 900 °C, and very similar to the double gyroidal carbons, it decreased to less than 35% after pyrolysis at 1600 °C (Table 2). Pore volumes

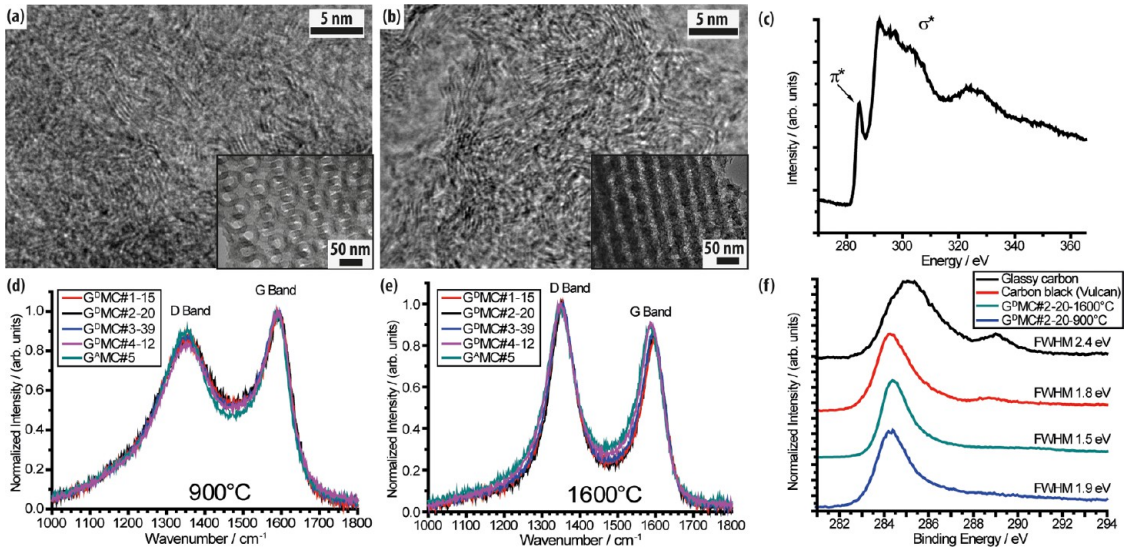

Figure 5. High-resolution transmission electron microscopy (HR-TEM) images of (a) G^{D}MC#2−20−1600 and (b) G^{A}MC#5−1600. Insets at a lower magnification of the same samples show the mesostructure. (c) Electron energy loss spectrum (EELS) of the carbon K-edge of G^{D}MC#2−20−1600. The spectrum is an average of six area spectra (10 × 10 nm^2) taken at different spots of the sample. Raman spectra of powders of double gyroidal mesoporous carbons pyrolyzed at (d) 900 °C and (e) 1600 °C showing the evolution of the D- and G-bands. (f) High-resolution X-ray photoelectron spectroscopy (HR-XPS) data of the carbon K-edge of G^{D}MC#2−20−900, G^{D}MC#2−20−1600, and for comparison, glassy carbon as well as carbon black, showing the decrease of the peak width at higher carbonization temperatures.

of 2.01 and 1.41 $cm^3\ g^{-1}$ for samples treated at 900 and 1600 °C, respectively, were observed by nitrogen sorption. These values exceeded the highest obtained pore volume for the double gyroidal morphology and corresponded to porosities of 80 and 74%, respectively. As seen for the double gyroidal morphology, this high pore volume was almost exclusively constituted by the mesopores after carbonization at 1600 °C. The micropore volume decreased by a factor of 3 upon pyrolysis at 1600 °C. The pore size distribution, calculated using the BJH model for cylindrical pores, showed a broad peak centered at 35 nm, with higher peak area for the sample heat-treated at 900 °C, in agreement with the higher pore volume (Figure 4c, inset). The pores of the single gyroidal carbon network do not exhibit cylindrical shape, as assumed in the BJH model, which can explain the large discrepancy between the pore size obtained from SEM image analysis and the BJH result.

Characterization of the Carbon Microstructure. In order to investigate their composition, atomic structure, and degree of graphitization, the ordered mesoporous carbon materials reported here were characterized by X-ray photoelectron spectroscopy (XPS), high-resolution XPS (HR-XPS), Raman spectroscopy, high-resolution TEM (HR-TEM), wide-angle X-ray diffraction (WAXD), and electron energy loss spectroscopy (EELS).

XPS can be used to investigate the elemental composition of the top 1−10 nm of a material. Since our materials showed wall thicknesses of less than 20 nm, we assume that the resulting elemental composition is representative for our bulk material. The carbon materials heated to 900 °C showed oxygen contents of 10−20% which decreased to 7−16% for materials pyrolyzed at 1600 °C (Table 2). The oxygen content was most likely due to hydroxyl groups on the carbon surface. In comparison, from XPS spectra of glassy carbon and carbon black (Vulcan X72), we calculated oxygen contents of 19 and 5%, respectively. The HR-XPS spectra of the carbon K-edge of G^{D}MC#2−20 carbonized at 900 and 1600 °C are shown in Figure 5f together with other carbon materials for comparison. HR-XPS showed one narrow peak centered at 284.4 eV, indicating that only one type of carbon was predominantly present. The full width at half-maximum (fwhm) of this G^{D}MC peak decreased with increasing carbonization temperature and was narrower than carbon black when pyrolyzed at 1600 °C. Furthermore, the carbon K-edge in EELS showed the appearance of a prepeak, due to the π^*-band, only present in sp^2-hybridized carbon materials (Figure 5c). We concluded from the HR-XPS and EELS spectra that, after carbonization at 1600 °C, the carbon atoms in the structured mesoporous materials were almost entirely sp^2-hybridized.

In order to determine the degree of graphitization, Raman spectroscopy and WAXD were applied to elucidate the in-plane size of the graphitic clusters and the number of stacked sheets, respectively. In Raman spectroscopy of disordered carbon materials, two bands, called the D- and the G-band, are typically observed at approximately 1350 and 1590 cm^{-1}, respectively. The G-band arises from the in-plane vibration of C═C double bonds, while the D-band is caused by a breathing mode of isolated benzene rings.[39] The Raman spectra of the G^{D}MC materials heated to

900 and 1600 °C are displayed in Figure 5d,e, respectively. For the two temperatures, the D- and the G-band were clearly visible at 1352 and 1592 cm^{-1} (900 °C) and 1352 and 1595 cm^{-1} (1600 °C), indicating the presence of disordered carbon. For a given pyrolysis temperature, the different G^DMC materials displayed identical Raman spectra irrespective of their pore size. Higher pyrolysis temperatures led to narrower bands and increased the ratio of the integrated intensities of the G-band to the D-band, suggesting a higher degree of graphitization for higher pyrolysis temperatures. Tuinstra and Koenig reported an empirical formula for the determination of the in-plane size of graphitic clusters based on the ratio of the G-band to the D-band (see Supporting Information).[39,40] Applying this formula, the in-plane size of the graphitic clusters was estimated to approximately 2.7 nm for the G^DMC-900 materials and to approximately 3.7 nm for the G^DMC-1600 materials (Table 2), consistent with values reported in the literature on the pyrolysis of phenolic resins.[41] In WAXD measurements of graphitic materials, the peak at 2θ = 23−27° corresponds to the (200) plane of graphite. The position of the peak depends on the spacing between the graphene sheets (2θ = 26.6° for graphite corresponding to 0.335 nm sheet spacing), and its fwhm gives information about the number of stacked graphene sheets. Measurements of the G^DMC materials yielded diffractograms with poorly defined peaks at 2θ = 25° (Figure S4). This indicated a small number of stacked graphene sheets but made an analysis of the fwhm of the peak unreliable.

HR-TEM images of G^DMC#2−20−1600 and G^AMC-1600 were consistent with the calculations from the Raman spectra (Figure 5a,b). Areas with four to eight parallel graphitic sheets of 3−5 nm length were observed. The orientation of the graphitic sheets in the different clusters was random and in no relationship to the features of the mesostructure, for example, parallel or vertical to the pore wall. Additionally, curvature is evident in most of the graphitic sheets. The small cluster size, random orientation, and varying curvature give rise to poor crystallographic long-range order. The lack of long-range order of more than a few nanometers is consistent with the poorly defined peaks observed in WAXD. Our analysis suggests that the microstructure of the gyroidal mesoporous carbons bears a strong resemblance to the microstructure of glassy carbon. The electrical conductivity of powdered gyroidal carbon materials was measured using a home-built four-point probe apparatus with uniaxial applied pressure of 250 psi as described in detail before.[42] The conductivities of G^DMC#2−20−900 and G^DMC#2−20−1600 were 0.1 and 2.1 S cm^{-1}, respectively, which makes our high-temperature-treated gyroidal mesoporous carbon comparable to carbon black (Vulcan XC72) with a measured conductivity of 4.2 S cm^{-1} under the same conditions.

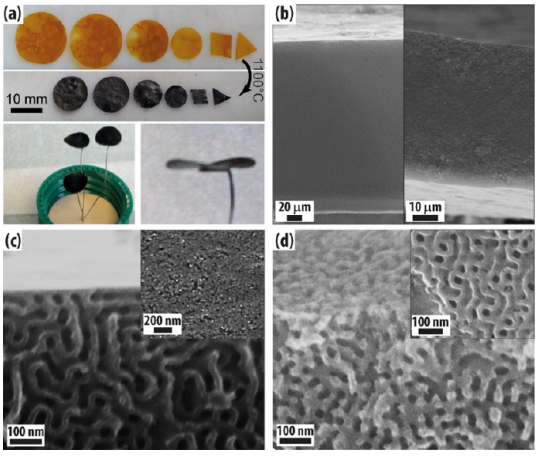

Figure 6. (a) Photographs of G^DMC#3−39−1200 monoliths from the top (bottom left) and conductively connected to silver wires (top left and right). Cross sectional SEM images of G^DMC#3−39−1200 monoliths of (b, left) 200 μm and (b, right) 50 μm thickness; higher magnification images at the edge of the surface (c) unexposed and (d) exposed to prior plasma treatment of the organic−organic hybrid. The insets in (c) and (d) show SEM images of the top surfaces only.

In order to elucidate the influence of the morphology on the graphitic cluster size, we investigated carbon materials from hybrids with hexagonally packed cylindrical morphology (see Supporting Information). Hybrids using ISO#1 and ISO#2 formed an inverse hexagonally packed cylindrical morphology at resols/ISO loadings up to 1.2:1 (Figure S5a). The materials showed similar Raman spectra as the gyroidal mesoporous carbons (Figure S5c). HR-TEM images also suggested randomly oriented graphitic clusters with the same apparent size and curvature as in the gyroidal materials (Figure S5d). This result suggests that, for the present terpolymer-derived carbons, there is no relationship between the carbon micro- and mesostructure. Formation of a well-defined hexagonally oriented cylindrical morphology at higher resols loadings demonstrated further structural tunability of mesoporous carbons *via* our synthesis procedure.

Monolithic Gyroidal Mesoporous Carbon. Following our synthesis strategy, we were able to synthesize monolithic gyroidal mesoporous carbons (mG^DMC) with tailored macroscopic dimensions. As-cast, annealed organic−organic hybrid films were flexible and therefore could be cut or punched into the desired shape (Figure 6a). After carbonization at temperatures up to 1600 °C, the monoliths retained their macroscopic appearance (Figure 6a). The large mesostructural shrinkage of 30% during heat treatment was translated into a macroscopic shrinkage of the monoliths (*e.g.*, a hybrid disc of 10 mm diameter yielded a gyroidal carbon monolith of 7 mm diameter, Figure 6a). Considering this large shrinkage, it was surprising that the monoliths kept their structural integrity without cracking or pulverizing. Furthermore, by altering the amount of material per casting area, we were able to tailor the

monolith thickness from over 200 μm to less than 50 μm, a thickness ideally suited for electrode applications (Figure 6b). The remarkable macrostructure preservation for different monolith sizes demonstrated the high versatility of our process. We attribute the macroscopic stability of the materials at high temperatures to the wall thickness of more than 10 nm as well as the bicontinuous mesostructure that allowed isotropic strain release during the shrinkage and assured sufficient release of the decomposition gases without building up of pressure inside the material that would cause cracking of the monolith. To the best of our knowledge, this is the first report of silica-free, soft-templated-ordered mesoporous carbon monoliths without macropores.

Moreover, we developed a procedure to fabricate monoliths with structured surfaces that show narrow pore size distributions (Figure 6c,d). A common problem with continuous films of mesostructured materials obtained by soft templating is the orientation of the pores and an unstructured or closed surface layer on the top and bottom of the film (see Figure 6c, inset, and Figure S1d) due to lamellar capping layers.[14,30] This is caused by the different surface energies of the various block copolymer domains during the casting process. Due to the bicontinuous nature of the cubic, gyroidal morphology, the orientation of the structure with respect to the surfaces is irrelevant. By oxygen/argon plasma etching of the organic–organic hybrid monoliths, the lamellar capping layers could be removed and the gyroidal bulk structure became directly accessible from the surface (see Figure 6d and inset). After carbonization at temperatures as high as 1600 °C, the surface showed gyroidal features, assuring a narrow pore size distribution also at the surface. The pores on the surface are slightly smaller according to SEM image analysis compared to the interior gyroidal porosity, however, most likely due to condensation of the polymeric materials on the surface during plasma treatment. Additionally, this simple process allows for selective exposure of only a fraction of the surface to the plasma, hence leading to a tailored opening of surface sites. For example, we covered one surface of a hybrid film during plasma treatment, which led to a carbon monolith with one closed surface and one ordered porous surface (similar to Figure 6c,d, respectively). Furthermore, this opened up the possibility of conductively connecting the monolith with silver or carbon paste on the closed side, making the monolith accessible for further electrochemical treatments, without the risk of the required binder to infiltrate the pores and, as a result, distort the measurements.

CONCLUSION

In this report, we have demonstrated the metal- and halogen-free synthesis of highly ordered double gyroidal mesoporous carbons, with tailored pore sizes of up to 39 nm, the largest reported pore size for soft-templated OMCs to date. By modification of the carbon precursor, to the best of our knowledge for the first time, we synthesized single gyroidal carbon networks form organic–organic hybrids with alternating gyroid morphology. Through the rational design of the triblock terpolymers, we show high tunability of the porosity between 32 and 80 vol % combined with structural stability up to 1600 °C, unprecedented for soft-templated-ordered mesoporous materials, ensuring a high degree of sp^2-hybridization and low microporosity with a glassy carbon-like microstructure. Finally, we demonstrated the first silica-free soft-templating process to fabricate monolithic gyroidal mesoporous carbons with tailored macroscopic shape and accessible surface pores through plasma treatment of the organic–organic hybrids before carbonization.

Since all the microstructural characteristics of the four reported double gyroidal mesoporous carbons are very similar to each other, this system is ideal for studies of the pore size dependence of the performance of such mesoporous carbon electrodes in energy technology or catalysis. Furthermore, the large and uniform pore size together with pore interconnectivity and the ability of making tailored monolithic materials thereof opens up new possibilities for the fabrication of functional multicomponent composites on the nanoscale, as illustrated on the right of Scheme 1.

METHODS

Synthesis. Five poly(isoprene)-*block*-poly(styrene)-*block*-poly(ethylene oxide) (ISO) terpolymers were synthesized *via* sequential anionic polymerization as described before.[32] Results on molar mass, composition, and polydispersity index (PDI) are summarized in Table 1. Polymer molar masses vary from 27 up to 108 kg mol^{-1}. Polydispersity indices were all below 1.1, demonstrating high control over the terpolymer synthesis.

Oligomeric phenol–formaldehyde resols with a molar mass of less than 500 g mol^{-1} were synthesized using the well-known polymerization of phenol and formaldehyde under basic conditions and worked up in a modified way compared to what has been previously described.[15] In a typical synthesis, 9.411 g of phenol (0.1 mol, redistilled, 99+%, Sigma-Aldrich) was melted in a three-neck flask equipped with a reflux condenser in a water bath at 45 °C. A 20 wt % sodium hydroxide solution was prepared by dissolution of 0.4 g of sodium hydroxide (0.01 mol, pellets, Mallinckrodt) in 1.6 g of deionized water. The sodium hydroxide solution was added dropwise to the melted phenol. The sodium phenoxide solution was stirred for 10 min and 14.89 mL of formalin solution (37 wt % in water, ACS Reagent, Sigma-Aldrich), containing 0.2 mol formaldehyde, was carefully added dropwise over 10 min. The slightly orange-colored solution was heated to 75 °C and held at this temperature for 1 h. The orange solution was allowed to cool to room temperature and subsequently neutralized with *para*-toluene sulfonic acid (≥98.5%, ACS reagent, Sigma-Aldrich). The orange/yellow

solution was freeze-dried overnight on a vacuum line, and the orange resols were dissolved in a mixture of tetrahydrofuran (Anhydrous, inhibitor free, ≥99.9%, Sigma-Aldrich) and chloroform (anhydrous, ≥99%, Sigma-Aldrich) (1:1 wt). The resulting cloudy solution was filtered through a PTFE syringe filter (0.2−0.4 μm) to remove the precipitated sodium *para*-toluene sulfonate, dried again overnight on a vacuum line, and dissolved in tetrahydrofuran/chloroform (1:1 wt) as a 25 wt % solution. Oligomeric resorcinol−formaldehyde resols were synthesized in a similar way. A highly concentrated resorcinol solution in water was used (50 wt %) and mixed with a 20 wt % sodium hydroxide solution and formalin solution. The molar ratio of resorcinol/NaOH/formaldehyde was 1:0.1:1. The mixture was stirred for 10 min at room temperature and promptly neutralized with *para*-toluene sulfonic acid. The red solution was freeze-dried overnight on a vacuum line, and the solid resorcinol−formaldehyde resols were dissolved in tetrahydrofuran. The resulting cloudy solution was filtered through a PTFE syringe filter (0.2−0.4 μm) to remove the precipitated sodium *para*-toluene sulfonate and higher molar mass resins, dried again overnight on a vacuum line, and dissolved in tetrahydrofuran as a 20 wt % solution. The molar mass of the synthesized resorcinol−formaldehyde resols was larger than the phenol based resols as indicated by a shorter elution time in gel permeation chromatography. However, the elution time was slightly longer than of a poly(styrene) standard with a molar mass of 1010 g mol^{-1}, indicating a smaller hydrodynamic radius than the poly(styrene) standard.

Organic−organic hybrids were synthesized through evaporation-induced self-assembly (EISA). The prepared resols solution was added to solutions of the ISO terpolymers in a 1:1 weight mixture of tetrahydrofuran and chloroform, yielding a 4−10 wt % solution and stirred for 24 h in the case of phenol−formaldehyde resols and 1 h in the case of resorcinol−formaldehyde resols. The ratios of resols to ISO to obtain the desired gyroidal morphology are summarized in Table 1. The solutions were cast in a Teflon dish at 50 °C covered with a glass dome to ensure a solvent saturated atmosphere throughout the drying process and subsequently cured at 110−130 °C in a convection oven for 24 h. For carbonization, the cured hybrids were heated at 1 °C min^{-1} to 600 °C and pyrolyzed under inert atmosphere (nitrogen or argon) at 600 °C for 3 h and then brought to the final temperature (see text) at a rate of 5 °C min^{-1}.

Monolithic double gyroidal carbons (mG^{D}MC) were fabricated by cutting the cured organic−organic hybrid monoliths into the desired shape and subsequent heat treatment as described above. For carbon monoliths with open and structured surfaces, the hybrid monoliths were exposed to oxygen/argon plasma for 30−60 min before carbonization.

Characterization. The composition of the triblock terpolymers was calculated using ^{1}H nuclear magnetic resonance (^{1}H NMR) spectroscopy. The polymers were dissolved in deuterated chloroform (chloroform-*d*, 99.8 atom % D, Aldrich) with a concentration of 15−20 mg mL^{-1}. ^{1}H NMR spectra were recorded on a Varian Mercury spectrometer at 300 MHz.

Gel permeation chromatography (GPC) was used to determine the molar mass of the triblock terpolymers and the oligomeric resols. Samples were prepared in tetrahydrofuran (THF) with a concentration of 1.5 mg mL^{-1}. GPC measurements were performed in THF at 23 °C (1 mL min^{-1}) on a Waters ambient-temperature GPC system equipped with a Waters 2410 differential refractive index (RI) detector.

The morphology of the organic−organic composites and porous carbon materials were determined using a combination of small-angle X-ray scattering, bright-field transmission electron microscopy, and scanning electron microscopy.

TEM samples of composite films were prepared by cryo-ultramicrotoming to a thickness of 50−70 nm using a Leica Ultracut UCT cryo-ultramicrotome equipped with a diamond knife at −60 °C. The microtomed sections were floated on a water/DMSO (40:60 vol) mixture and subsequently placed on copper grids. Contrast was obtained by staining the samples with osmium tetroxide vapor (60 min). Heat-treated porous materials were crushed in a ball mill, dispersed in ethanol, and dropped onto carbon-coated copper grids. Bright-field transmission electron microscopy was performed on a FEI Tecnai T-12 TWIN TEM operating at an accelerating voltage of 120 kV equipped with a high-resolution, thermoelectrically cooled Gatan Orius dual-scan CCD camera. HR-TEM images were obtained on a FEI-F20-TEM-STEM operating at an accelerating voltage of 200 kV. Scanning electron microscopy of carbonized samples was carried out on a Zeiss LEO 1550 FE-SEM operating at an accelerating voltage of 10 kV. Due to the conductivity of the samples, no additional coating of the specimen was necessary.

For SAXS measurements, small squares of the cured composites and pyrolyzed films (*ca.* 2 × 2 mm^2) were cut and placed in the hole of a metal washer that was covered on one side with Kapton tape. SAXS measurements were performed at the Cornell High Energy Synchrotron Source (CHESS). The sample to detector distance was 2.6 m, and the X-ray wavelength was 1.2015 Å. The scattering vector q is defined as $q = (4\pi/\lambda)\sin\theta$, where θ is half of the scattering angle.

X-ray diffraction patterns were obtained on an Ultima IV multipurpose X-ray diffraction system from Rigaku using Cu Kα radiation (40 V, 44 mA, wavelength 1.5418 Å) in a 2θ range between 10 and 90° with a speed of 5° min^{-1}.

For Raman spectroscopy, a Renishaw InVia confocal Raman microscope was used at room temperature in a backscattering geometry, equipped with a 488 nm diode laser as an excitation source focused on the sample with a 50× magnification.

Sorption isotherms were obtained on a Micromeritics ASAP 2020 surface area and porosity analyzer at −196 °C. The samples were degassed at 200 °C under vacuum for at least 10 h prior to measurements. The specific surface areas were determined using the Brunauer−Emmett−Teller (BET) method. Pore size distributions were calculated using the Barrett−Joyner−Halenda (BJH) method.[34,35]

Conflict of Interest: The authors declare no competing financial interest.

Acknowledgment. This work was supported as part of the Energy Materials Center at Cornell (emc^2), an Energy Frontier Research Center funded by the U.S. Department of Energy, Office of Science, Basic Energy Sciences under Award No. DE-SC0001086. T.N.H. thanks the Swiss National Science Foundation (SNF) for a Postdoc fellowship. This work made use of the Cornell Center for Materials Research Shared Facilities which are supported through the NSF MRSEC program (DMR-1120296). This work was further based upon research conducted at the Cornell High Energy Synchrotron Source (CHESS) which is supported by the National Science Foundation and the National Institutes of Health/National Institute of General Medical Sciences under NSF Award DMR-0936384. The authors also gratefully acknowledge Prof. D. Muller and B. Levin of Cornell University for helpful discussions and kind experiment assistance with the EELS measurements.

Supporting Information Available: Further electron microscopy, nitrogen sorption, and X-ray scattering analysis is provided. A detailed description of the Raman analysis and the characterization data of inverse hexagonally packed carbon cylinders are provided. This material is available free of charge *via* the Internet at http://pubs.acs.org.

REFERENCES AND NOTES

1. Bansal, R. C.; Donnet, J. B.; Stoeckli, F. *Active Carbon*; Marcel Dekker: New York, 1988.
2. Yang, R. T. *Adsorbents: Fundamentals and Applications*; Wiley-Interscience: New York, 2003.
3. Gaffney, T. R. Porous Solids for Air Separation. *Curr. Opin. Solid State Mater. Sci.* **1996**, *1*, 69–75.
4. Ryoo, R.; Joo, S. H.; Jun, S. Synthesis of Highly Ordered Carbon Molecular Sieves *via* Template-Mediated Structural Transformation. *J. Phys. Chem. B* **1999**, *103*, 7743–7746.
5. Lee, J.; Yoon, S.; Hyeon, T.; Oh, S. M.; Kim, K. B. Synthesis of a New Mesoporous Carbon and Its Application to Electrochemical Double-Layer Capacitors. *Chem. Commun.* **1999**, 2177–2178.

6. Tian, B. Z.; Che, S. N.; Liu, Z.; Liu, X. Y.; Fan, W. B.; Tatsumi, T.; Terasaki, O.; Zhao, D. Y. Novel Approaches To Synthesize Self-Supported Ultrahin Carbon Nanowire Arrays Templated by MCM-41. *Chem. Commun.* **2003**, 2726–2727.
7. Jun, S.; Joo, S. H.; Ryoo, R.; Kruk, M.; Jaroniec, M.; Liu, Z.; Ohsuna, T.; Terasaki, O. Synthesis of New, Nanoporous Carbon with Hexagonally Ordered Mesostructure. *J. Am. Chem. Soc.* **2000**, *122*, 10712–10713.
8. Che, S. N.; Garcia-Bennett, A. E.; Liu, X. Y.; Hodgkins, R. P.; Wright, P. A.; Zhao, D. Y.; Terasaki, O.; Tatsumi, T. Synthesis of Large-Pore *Ia3d* Mesoporous Silica and Its Tubelike Carbon Replica. *Angew. Chem., Int. Ed.* **2003**, *42*, 3930–3934.
9. Liu, X. Y.; Tian, B. Z.; Yu, C. Z.; Gao, F.; Xie, S. H.; Tu, B.; Che, R. C.; Peng, L. M.; Zhao, D. Y. Room-Temperature Synthesis in Acidic Media of Large-Pore Three-Dimensional Bicontinuous Mesoporous Silica with *Ia3d* Symmetry. *Angew. Chem., Int. Ed.* **2002**, *41*, 3876–3878.
10. Kleitz, F.; Choi, S. H.; Ryoo, R. Cubic *Ia3d* Large Mesoporous Silica: Synthesis and Replication to Platinum Nanowires, Carbon Nanorods and Carbon Nanotubes. *Chem. Commun.* **2003**, 2136–2137.
11. Kim, T. W.; Kleitz, F.; Paul, B.; Ryoo, R. MCM-48-like Large Mesoporous Silicas with Tailored Pore Structure: Facile Synthesis Domain in a Ternary Triblock Copolymer–Butanol–Water System. *J. Am. Chem. Soc.* **2005**, *127*, 7601–7610.
12. Yang, H. F.; Shi, Q. H.; Liu, X. Y.; Xie, S. H.; Jiang, D. C.; Zhang, F. Q.; Yu, C. Z.; Tu, B.; Zhao, D. Y. Synthesis of Ordered Mesoporous Carbon Monoliths with Bicontinuous Cubic Pore Structure of *Ia3d* Symmetry. *Chem. Commun.* **2002**, 2842–2843.
13. Liang, C. D.; Hong, K. L.; Mays, J. W.; Dai, S. Synthesis of a Large-Scale Highly Ordered Porous Carbon Film by Self-Assembly of Block Copolymers. *Angew. Chem., Int. Ed.* **2004**, *43*, 5785–5789.
14. Tanaka, S.; Nishiyama, N.; Egashira, Y.; Ueyama, K. Synthesis of Ordered Mesoporous Carbons with Channel Structure from an Organic–Organic Nanocomposite. *Chem. Commun.* **2005**, 2125–2127.
15. Meng, Y.; Gu, D.; Zhang, F. Q.; Shi, Y. F.; Cheng, L.; Feng, D.; Wu, Z. X.; Chen, Z. X.; Wan, Y.; Stein, A.; *et al.* A Family of Highly Ordered Mesoporous Polymer Resin and Carbon Structures from Organic–Organic Self-Assembly. *Chem. Mater.* **2006**, *18*, 4447–4464.
16. Liu, L. W.; Wang, F.-Y.; Shao, G.-S.; Ma, T.-Y.; Zhong, Z.-Y. Synthesis of Ultra-large Mesoporous Carbons from Triblock Copolymers and Phloroglucinol/Formaldehyde Polymer. *Carbon* **2010**, *9*, 2660–2664.
17. Fulvio, P. F.; Mayes, R. T.; Wang, X.; Mahurin, S. M.; Bauer, J. C.; Presser, V.; McDonough, J.; Gogotsi, Y.; Dai, S. "Brick-and-Mortar" Self-Assembly Approach to Graphitic Mesoporous Carbon Nanocomposites. *Adv. Funct. Mater.* **2011**, *21*, 2208–2215.
18. Kosonen, H.; Valkama, S.; Nykanen, A.; Toivanen, M.; ten Brinke, G.; Ruokolainen, J.; Ikkala, O. Functional Porous Structures Based on the Pyrolysis of Cured Templates of Block Copolymer and Phenolic Resin. *Adv. Mater.* **2006**, *18*, 201–205.
19. Deng, Y.; Yu, R.; Wan, X.; Shi, Y.; Meng, Y.; Gu, D.; Zhang, L.; Huang, Y.; Liu, C.; Wu, X.; *et al.* Ordered Mesoporous Silicas and Carbons with Large Accessible Pores Templated from Amphiphilic Diblock Copolymer Poly(ethylene oxide)-*b*-Polystyrene. *J. Am. Chem. Soc.* **2007**, *129*, 1690–1697.
20. Zhang, J.; Deng, Y.; Wei, J.; Sun, Z.; Gu, D.; Bongard, H.; Liu, C.; Wu, H.; Tu, B.; Schüth, F.; *et al.* Design of Amphiphilic ABC Triblock Copolymer for Templating Synthesis of Large-Pore Ordered Mesoporous Carbons with Tunable Pore Wall Thickness. *Chem. Mater.* **2009**, *21*, 3996–4005.
21. Wei, J.; Deng, Y.; Zhang, J.; Sun, Z.; Tu, B.; Zhao, D. Y. Large-Pore Ordered Mesoporous Carbons with Tunable Structures and Pore Sizes Templated from Poly(ethylene oxide)-*b*-Poly(methyl methacrylate). *Solid State Sci.* **2011**, *13*, 784–792.
22. Li, J.-G.; Lin, Y.-D.; Kuo, S.-W. From Microphase Separation to Self-Organized Mesoporous Phenolic Resin through Competitive Hydrogen Bonding with Double-Crystalline Diblock Copolymers of Poly(ethylene oxide-*b*-ε-caprolactone). *Macromolecules* **2011**, *44*, 9295–9309.
23. Deng, Y.; Liu, J.; Liu, C.; Gu, D.; Sun, Z.; Wei, J.; Zhang, J.; Zhang, L.; Tu, B.; Zhao, D. Y. Ultra-large-Pore Mesoporous Carbons Templated from Poly(ethylene oxide)-*b*-Polystyrene Diblock Copolymer by Adding Polystyrene Homopolymer as a Pore Expander. *Chem. Mater.* **2008**, *20*, 7281–7286.
24. Wang, X.; Liang, C.; Dai, S. Facile Synthesis of Ordered Mesoporous Carbons with High Thermal Stability by Self-Assembly of Resorcinol–Formaldehyde and Block Copolymers under Highly Acidic Conditions. *Langmuir* **2008**, *24*, 7500–7505.
25. Huang, Y.; Cai, H. Q.; Feng, D.; Gu, D.; Deng, Y. H.; Tu, B.; Wang, H. T.; Webley, P. A.; Zhao, D. Y. One-Step Hydrothermal Synthesis of Ordered Mesostructured Carbonaceous Monoliths with Hierarchical Porosities. *Chem. Commun.* **2008**, 2641–2643.
26. Liang, C. D.; Dai, S. Dual Phase Separation for Synthesis of Bimodal Meso-/Macroporous Carbon Monoliths. *Chem. Mater.* **2009**, *21*, 2115–2124.
27. Mayes, R. T.; Tsouris, C.; Kiggans, J. O.; Mahurin, S. M.; DePaoli, D. W.; Dai, S. Hierarchical Ordered Mesoporous Carbon from Phloroglucinol-Glyoxal and Its Applications in Capacitive Deionization of Brackish Water. *J. Mater. Chem.* **2010**, *20*, 8674–8678.
28. Hao, G. P.; Li, W. C.; Qian, D.; Wang, G. H.; Zhang, W. P.; Zhang, T.; Wang, A. Q.; Schüth, F.; Bongard, H. J.; Lu, A. H. Structurally Designed Synthesis of Mechanically Stable Poly(benzoxazine-*co*-resol)-Based Porous Carbon Monoliths and Their Application as High-Performance CO_2 Capture Sorbents. *J. Am. Chem. Soc.* **2011**, *133*, 11378–11388.
29. Hao, G. P.; Li, W. C.; Wang, S. A.; Wang, G. H.; Qi, L.; Lu, A. H. Lysine-Assisted Rapid Synthesis of Crack-Free Hierarchical Carbon Monoliths with a Hexagonal Array of Mesopores. *Carbon* **2011**, *49*, 3762–3772.
30. Wei, H.; Lv, Y.; Han, L.; Tu, B.; Zhao, D. Y. Facile Synthesis of Transparent Mesostructured Composites and Corresponding Crack-free Mesoporous Carbon/Silica Monoliths. *Chem. Mater.* **2011**, *23*, 2353–2360.
31. Stefik, M.; Wang, S.; Hovden, R.; Sai, H.; Tate, M. W.; Muller, D. A.; Steiner, U.; Gruner, S. M.; Wiesner, U. Networked and Chiral Nanocomposites from ABC Triblock Terpolymer Coassembly with Transition Metal Oxide Nanoparticles. *J. Mater. Chem.* **2012**, *22*, 1078–1087.
32. Bailey, T. S.; Hardy, C. M.; Epps, T. H.; Bates, F. S.; Noncubic Triply, A. Periodic Network Morphology in Poly(isoprene-*b*-styrene-*b*-ethylene oxide) Triblock Copolymers. *Macromolecules* **2002**, *35*, 7007–7017.
33. Florent, M.; Xue, C.; Zhao, D. Y.; Goldfarb, D. Formation Mechanism of Cubic Mesoporous Carbon Monolith Synthesized by Evaporation-Induced Self-Assembly. *Chem. Mater.* **2012**, *24*, 383–392.
34. Gregg, S. J.; Sing, K. S. W. *Adsorption, Surface Area and Porosity*, 2nd ed.; Academic Press: London, 1982.
35. Barrett, E. P.; Joyner, L. G.; Halenda, P. P. The Determination of Pore Volume and Area Distributions in Porous Substances. *J. Am. Chem. Soc.* **1951**, *73*, 373–380.
36. Toombes, G.; Finnefrock, A.; Tate, M. W.; Ulrich, R.; Wiesner, U.; Gruner, S. A Re-evaluation of the Morphology of a Bicontinuous Block Copolymer–Ceramic Material. *Macromolecules* **2007**, *40*, 8974–8982.
37. Epps, T. H.; Cochran, E. W.; Bailey, T. S.; Waletzko, R. S.; Hardy, C. M.; Bates, F. S. Ordered Network Phases in Linear Poly(isoprene-*b*-styrene-*b*-ethylene oxide) Triblock Copolymers. *Macromolecules* **2004**, *37*, 8325–8341.
38. Leibler, L. Theory of Microphase Separation in Block Copolymers. *Macromolecules* **1980**, *13*, 1602–1617.
39. Ferrari, A. C.; Robertston, J. Interpretation of Raman Spectra of Disordered and Amorphous Carbon. *Phys. Rev. B* **2000**, *61*, 14095–14107.

40. Tuinstra, F.; Koenig, J. L. Raman Spectrum of Graphite. *J. Chem. Phys.* **1970**, *53*, 1126–1130.
41. Ko, T.-H.; Kuo, W.-S.; Chang, Y.-H. Raman Study of the Microstructure Changes of Phenolic Resin during Pyrolysis. *Polym. Compos.* **2000**, *21*, 745–750.
42. Subban, C. V.; Smith, I. C.; DiSalvo, F. J. Interconversion of Inverse Opals of Electrically Conducting Doped Titanium Oxides and Nitrides. *Small* **2012**, *8*, 2824–2832.